Combustion and Flame 254 (2023) 112832

Contents lists available at ScienceDirect

Combustion and Flame

journal homepage: www.elsevier.com/locate/combustflame

On the roles of humidification and radiation during the ignition of ammonia–hydrogen–air mixtures

Shu Zheng[a], Hao Liu[a], Yiqing Wang[c], Xinyi Chen[d], Ran Sui[b,*], Qiang Lu[a,*]

[a] National Engineering Research Center of New Energy Power Generation, North China Electric Power University, Beijing 102206, China
[b] Center for Combustion Energy and MoE Key Laboratory of Thermal Science and Power Engineering, Department of Energy and Power Engineering, Tsinghua University, Beijing 100084, China
[c] SKLTCS, CAPT, BIC-ESAT, College of Engineering, Peking University, Beijing 100871, China
[d] Institute for Simulation of reactive Thermo-Fluid Systems, TU Darmstadt, Otto-Berndt-Straße 2, 64287 Darmstadt, Germany

ARTICLE INFO

Article history:
Received 3 January 2023
Revised 23 April 2023
Accepted 3 May 2023

Keywords:
NH_3/H_2 combustion
Radiation
Reabsorption
Minimum ignition energy
Water content

ABSTRACT

It is well established that radiation plays an important role in the combustion process of premixed combustible mixtures, which significantly affects the flame temperature and chemical reaction rates during flame propagation. However, the impact of radiation, especially the radiation reabsorption effect, on minimum ignition energy (E_{min}) still lacks thorough research and understanding. In this study, the ignition processes of spherical $NH_3/H_2/H_2O/O_2/N_2$ flames were simulated. Three different computational models, the adiabatic model (ADI), the optically thin model (OTM) and the statistical narrow-band model (SNB), were employed to determine the radiation effect (including both radiative heat loss and reabsorption) on E_{min}. Results indicated that the water content in the premixture suppressed ignition; characteristically, the addition of vol. 9.63% H_2O in the premixture resulted in a nearly 40% increase of E_{min} under adiabatic condition. Both radiative heat loss and reabsorption effects increased E_{min}. The radiation effects on E_{min}, quantified as the relative differences between the OTM-/SNB- and ADI-obtained E_{min}, were up to 16.47% (for radiative heat loss) and 17.65% (for radiation reabsorption), respectively. It was further demonstrated that radiation increased E_{min} through the combination of three aspects: thermal effect, chemical effect and flame structure effect. The thermal effect, induced by the outward radiative emission, reduced the ignition kernel temperature significantly. The reduced temperature decelerated chemical reactions and then suppressed the chemical heat release, i.e., the chemical effect as reflected by the concentrations of H, O and OH radicals. Furthermore, the larger flame thickness obtained by the radiation models slowed down the diffusion of fuels, which weakened the chemical heat release and eventually increased the E_{min}. Moreover, the reaction-diffusion region simulated by SNB was enlarged due to the radiation reabsorption, and thus, E_{min} obtained by SNB was higher than that by OTM.

1. Introduction

With its easy storage and transportation, as well as new techniques for its clean and economic production [1], ammonia (NH_3) has been considered as an emerging renewable energy with zero carbon emission [2]. However, large-scale applications employing NH_3 as a fuel in current combustion engines are hindered by its narrow flammability limits [3], low flame speed [4], high minimum ignition energy [5] and NO_x emission [6]. Several studies indicated that hydrogen (H_2) blending could improve the ignition and combustion characteristics of NH_3, via reducing ignition energy [7], stabilizing flame [3] and enhancing laminar flame speed [8]. Meanwhile, as a convenient method for emission control, humidification of premixed reactants (namely H_2O addition), was attempted in NH_3/H_2 combustion to reduce NO_x emission [9]. The existence of H_2 and H_2O, particularly the latter, inevitably affects the ignition of NH_3 mixtures. Therefore, it is necessary to analyze how to achieve a feasible compromise between emission reduction and ignition inhibition.

Minimum ignition energy (E_{min}), defined as the minimum amount of energy required to ignite a specified mixture and maintain self-sustained flame propagation [10], is a vital parameter to evaluate the ignitability of combustible mixtures. Extensive experiments have been conducted to access E_{min} of NH_3 mixtures. Verkamp et al. [3] measured E_{min} of atmospheric NH_3/air mixtures with different dissociated degrees and reported 8 mJ E_{min} for pure NH_3 in air ($\phi = 0.9$), which was 16 times larger than that of propane under the same conditions. They also pointed out that

* Corresponding authors.
E-mail addresses: sui@tsinghua.edu.cn (R. Sui), qianglu@mail.ustc.edu.cn (Q. Lu).

https://doi.org/10.1016/j.combustflame.2023.112832
0010-2180/

partial dissociation significantly promoted ignition of NH_3/air mixtures; characteristically, NH_3 with 28 vol.% dissociation exhibited similar combustion properties as hydrocarbon fuels in gas turbine combustors. Subsequently, Takizawa et al. [11] measured E_{min} of NH_3 through quenching distance $d_{q,h}$ and maximum flame speed $S_{u0,max}$ of the simplified heat loss theory. Consistent with the conclusion of Verkamp et al. [3], the estimated E_{min} of NH_3 was an order of magnitude higher than that of propane. It is worth noting the inaccuracy of experimentally measured E_{min} was emphasized in their study: E_{min} of NH_3 fluctuated by up to two orders of magnitude (from 648.7 to 7.4 mJ) when the electrode gap was changed from 2 to 6 mm. To this direction, numerical simulations are recognized as a proper way to study the ignition process that can avoid measurement uncertainties caused by factors that are difficult to control precisely, such as electrode size, electrodes gas and spark duration [12], better capture the details during transient processes of ignition kernel growth, and quantify parameters that are difficult to measure accurately.

In terms of numerical studies on ignition energies, Wu et al. [13] preformed one-dimensional simulations of flame initiation for atmospheric-pressure methane/air and iso-octane/air mixtures, where the effects of ignition source geometry, ignition kernel radius and mixture composition on E_{min} were investigated. Two evolutions of ignition failure were observed, i.e., either reactions were not initiated, or the ignition kernel quenched rapidly after formation. Their results indicated that E_{min} of the two fuels both exhibited a U-shape dependence of equivalent ratio ϕ. However, the specific mechanisms determining E_{min} were not revealed in their study. Furthermore, Zhang et al. [14] investigated dilution effects on ignition processes and E_{min} of H_2/air mixtures with He, Ar, N_2 and CO_2 blending. Their results showed that CO_2 had the smallest dilution limit (dilution ratio above which the mixture cannot be ignited [14]) and the strongest inhibition on ignition among the diluents, not only due to its high heat capacity, but also its chemical effect during the ignition process. The thermal and flame-dynamic effects of different diluents were discussed and quantified by adiabatic flame temperatures and Markstein lengths, respectively. The thermal effect always inhibited ignition, while the flame-dynamics either promoted or suppressed ignition depending on the specific diluent. Subsequently, Lesmana et al. [7] carried out numerical simulations to elucidate the ignition process of partially dissociated NH_3 mixtures, with maximum 7.5 vol.% H_2 in the fuel, and reported that E_{min} was significantly decreased with higher degree of ammonia dissociation (i.e., with the increase of H_2). The flame kernel temperature, rate of production for key radicals and heat release rate played key roles in the determination of flame self-sustaining. Meanwhile, the effect of water vapor dilution on E_{min} was studied for methane, *n*-butane and *n*-decane flames by Zhang et al. [15], where the thermal, dilution and chemical effects were examined. They concluded that the increase of E_{min} due to the presence of water vapor was mainly achieved via reducing the flame temperature and changing the reaction rates. Generally, it is widely accepted that E_{min} is primarily affected by temperature and chemical reaction rate during an ignition process. However, the radiation effect, which has been recognized to significantly affect flame temperature and chemical reactions during flame propagation [16–18], has not been fully understood in the past investigations on E_{min} (especially for mixtures with H_2O and H_2 as mentioned above).

In this study, the radiation effect on E_{min} of spherical $NH_3/H_2/H_2O/O_2/N_2$ flames under different humidification conditions were assessed via numerical simulations. The paper is organized as follows: in Section 2, the numerical models and computational settings are detailed. In Section 3, the general effect of water addition on E_{min} is first discussed with cases under adiabatic condition, decoupling the radiation effect. Subsequently, the radiation effect on E_{min} is elaborated separately from the thermal, chemical and flame structure aspects. Finally, the main findings are summarized in Section 4.

2. Numerical models and simulation details

In this study, the ignition process of premixed spherical $NH_3/H_2/H_2O/O_2/N_2$ flames was simulated by the in-house code A-SURF (Adaptive Simulation of Unsteady Reactive Flow) in a one-dimensional spherical coordinate, using the finite volume method. The code has been widely validated and used in studies on initiation and propagation of spherical flames [19–23]. The accuracy of A-SURF on E_{min} prediction was verified in previous studies [14,15]. The detailed governing equations, numerical methods and code validation of A-SURF can be found in [21,24] and thus not repeated here. The flame ignition was achieved by spatial dependent energy deposition for a given ignition time

$$q_{ig}(r,t) = \begin{cases} \frac{E_{ig}}{\pi^{1.5} r_{ig}^3 \tau_{ig}} \exp\left[-\left(\frac{r}{r_{ig}}\right)^2\right] & if \quad t < \tau_{ig} \\ 0 & if \quad t \geq \tau_{ig} \end{cases} \tag{1}$$

where E_{ig} was the total ignition energy, τ_{ig} the duration of the energy source, and r_{ig} the ignition kernel radius. In this study, the computation domain of all simulations was $0 \leq r \leq 40$ cm, with the initial temperature $T_u = 423$ K at atmospheric pressure. To maintain adequate numerical resolution of the moving flame, a multi-level, dynamically and locally adaptive mesh refinement algorithm was adopted. Eight grid levels were utilized and the moving reaction zone was always fully covered by a mesh size of 16 μm. Zero flow velocity, zero gradients of temperature and mass fractions are enforced at the boundaries. Constant values of $\tau_{ig} = 400$ μs and $r_{ig} = 400$ μm were adopted to eliminated their effects on E_{min} [25]. A trial-and-error method with relative error below 2% was used to determine the E_{min}.

Three computational models: adiabatic model (ADI), the optically thin model (OTM) and the statistical narrow-band model (SNB), were employed to predict E_{min} and to reveal the radiation effects. The ADI model does not consider any radiation. The OTM only considers the external radiative heat loss from the flame and ignores the radiation emission and absorption inside the flame, which are, in contrast, taken into account comprehensively in the SNB model. Hence, the effects of radiation heat loss and radiation reabsorption can be quantified by the relative differences between OTM/ADI and OTM/SNB, respectively. In this study, the radiation effects of NH_3 and H_2O were taken into consideration. The Planck-mean absorption coefficients (PMACs) adopted in the OTM (calculated line-by-line, LBL) and the mean narrow band parameters adopted in the SNB (calculated by the Young's band model theory [26]) were developed based on the HITEMP 2010 database [27] for H_2O and HITRAN 2016 database [28] for NH_3, respectively. The accuracy and performance of the above radiation models in assessing radiative heat transfer have been validated in our previous studies [29–31].

The kinetic model developed by Shrestha et al. [32] for oxygen-enriched NH_3/H_2 mixtures was adopted in this study, which has been validated for H_2 contents up to 30 vol.% in the fuel. Compositions of the simulated premixed $NH_3/H_2/H_2O/O_2/N_2$ mixtures are provided in Table 1. NH_3:H_2 volumetric ratio $X_{NH3}/(X_{NH3}+X_{H2})$ was fixed at 7:3 and the equivalence ratio (considering NH_3 oxidized to N_2 and H_2O) was maintained at $\phi = 1.2$. To compare with literature experimental data of [9], four humidification contents were employed, i.e., 0, 3.43, 6.63 and 9.63 vol.% (denoted as Cases WL0-3), respectively. The composition of the initial mixture was specified according to the molar ratios given by

$$(1-a)\frac{\phi(0.7NH_3 + 0.3H_2) + 0.675(O_2 + 3.76N_2)}{\phi + 0.675 \times 4.76} + aH_2O \tag{2}$$

Table 1
Compositions of simulated $NH_3/H_2/H_2O/O_2/N_2$ mixtures (by mole).

Case	NH_3	H_2	H_2O	O_2	N_2
WL0	0.19029	0.08155	0.00000	0.15291	0.57525
WL1	0.18376	0.07876	0.03430	0.14767	0.55551
WL2	0.17767	0.07615	0.06630	0.14277	0.53711
WL3	0.17197	0.07370	0.09630	0.13819	0.51984

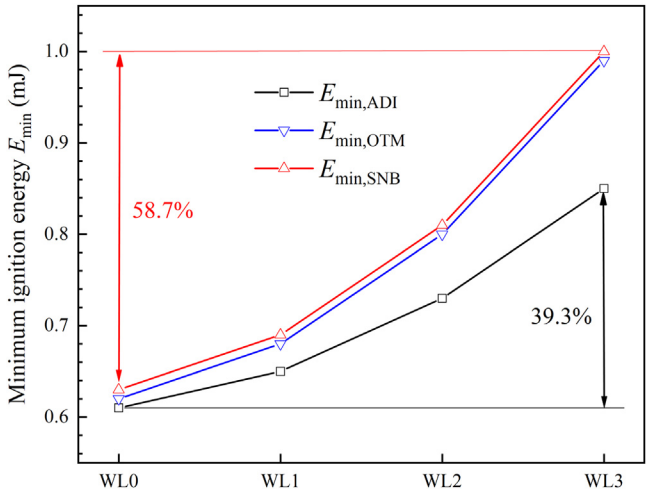

Fig. 1. Minimum ignition energy E_{min} calculated by ADI, OTM and SNB models for all the cases.

where a represents the humidification content (varied from 0 to 9.63%) and ϕ the equivalence ratio, which was fixed at 1.2 in this study.

3. Results and discussion

Figure 1 shows the minimum ignition energy E_{min} of the $NH_3/H_2/H_2O/O_2/N_2$ mixtures in Table 1 calculated by ADI, OTM and SNB models. It is observed that the E_{min} predicted by the three models all increased monotonically with rising water content, E_{min} results obtained via OTM were significantly greater than those of ADI and slightly lower than those of SNB. With the ADI model (i.e., under adiabatic condition without radiation, see the black line in Fig. 1), when the vol. water content was increased from 0 to 9.63%, E_{min} changed from 0.61 to 0.85 mJ, resulting in a 39.3% increase. In contrast, such increase for the OTM and SNB models, as shown with the blue and red lines, was amplified to nearly 60%, due to the consideration of radiation.

3.1. Humidification effect on E_{min}

To explore the effects of humidification on E_{min} and to decouple the radiation effect, the discussion based on ADI simulation were conducted firstly. The ignition processes of adiabatic $NH_3/H_2/H_2O/O_2/N_2$ mixtures with various degrees of humidification were simulated with a fixed E_{ig} 1.2 mJ, to avoid falsifications caused by different external energy inputs and to ensure ignition under all simulated conditions. Time evolutions of flame radius R_f, maximum heat release rate Q_{max} and maximum flame kernel temperature T_{max} are given in Fig. 2. As shown, T_{max} of all cases first increased quickly with the accumulated energy input (i.e., with time). When the ignition process was complete (at around t = 400 μs), T_{max} dropped until to the adiabatic temperature. Most reactions occurred before 100 μs were endothermic, while heat release started at t = ~120 μs and reached peak values at ~180 μs (see the curves of Q_{max}). Comparisons of time evolutions among

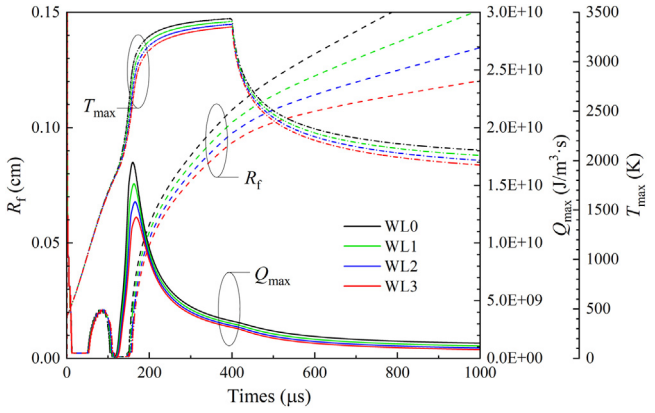

Fig. 2. Time evolutions of flame radius R_f, maximum temperature T_{max} and maximum heat release rate Q_{max} for the $NH_3/H_2/H_2O/O_2/N_2$ mixtures for all the cases.

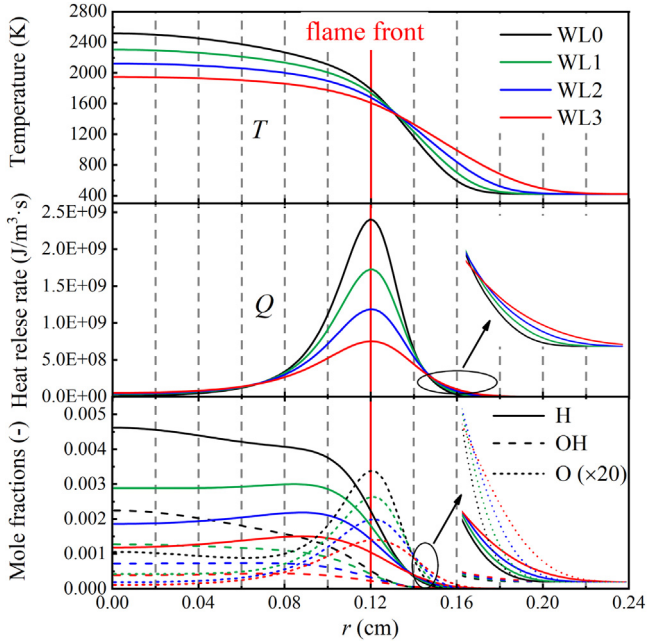

Fig. 3. Flame structures (distribution of temperature, chemical heat release rate and key radicals) for all the cases when R_f = 0.12 cm.

different humidification conditions indicated that T_{max} and Q_{max} (both the peak and stabilized values) decreased with increasing water content, which also significantly inhibited the propagation of the ignition kernel (see the flame radii R_f) and increased E_{min} (see Fig. 1).

Subsequently, to further reveal the impact of humidification on the initial flame transition [21], flame structures of Cases WL0-3 when their flame fronts propagated to the same location with radius R_f = 0.12 cm (at 496, 581, 724 and 1023 μs for WL0-3, respectively, when the external energy deposition was finished and the flame radius of each case was within the critical radius [21]) are compared in Fig. 3, which also includes the distributions of temperature, heat release rate and key radicals (H, OH and O). On the one hand, H_2O addition diluted NH_3 and H_2 and naturally suppressed the maximum flame kernel temperature (at the flame center, r = 0 cm) and heat release rate (see Q_{max} at the flame front r = 0.12 cm). On the other hand, the increased water content thickened the flame (detailed data are presented below), thus enlarged the reaction-diffusion zone (see the less steeper profiles for Q and the radicals in the zoomed-in subfigures of Fig. 3) and increased the temperature, heat release and radicals in the unburned zone

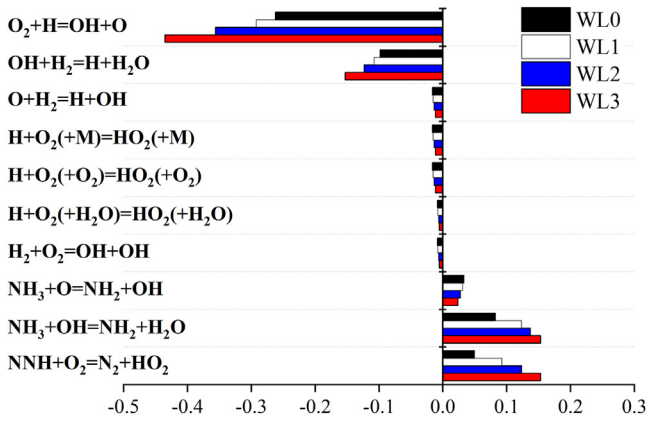

Fig. 4. Sensitivity coefficients of important reactions for E_{min} of all the cases.

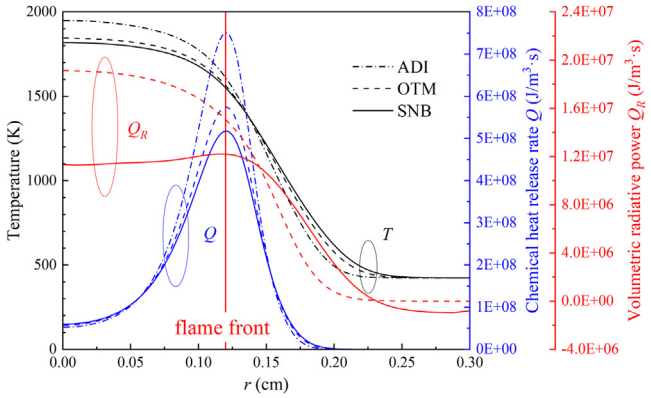

Fig. 5. Distributions of temperature T, heat release rate Q and volumetric radiative power Q_R calculated by ADI, OTM and SNB models for Case WL3 when $R_f = 0.12$ cm.

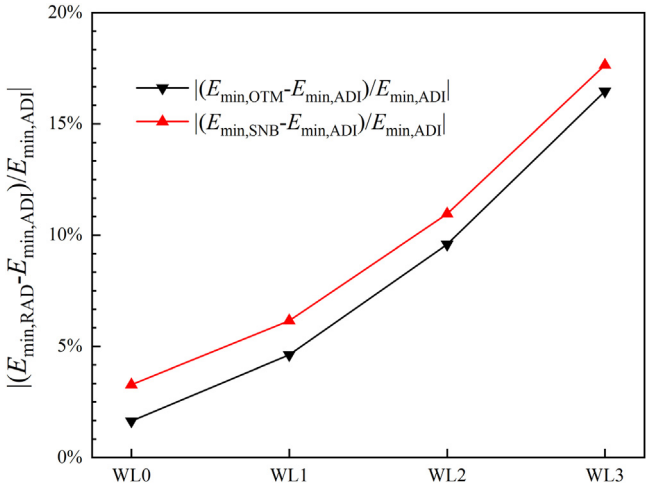

Fig. 6. Absolute relative differences of E_{min} between the two radiative models and the adiabatic model for all the cases.

(at approximately $r > 0.13$, 0.15 and 0.14 cm, respectively), eventually the fuel diffusion towards the reaction zone slowed down, and the temperatures at the flame center ($r = 0$ cm) and the reaction zone ($r = 0.12$ cm) were both reduced by the increased water contents in the mixture.

Furthermore, H_2O could directly (as reactant/product) and indirectly (as a three-body) affect the rates of chemical reactions [14], namely act on E_{min} through chemical effect. Sensitivity analysis for E_{min} was conducted for different humidification conditions. As shown in Fig. 4, the chain branching reaction $O_2 + H = OH + O$ had the largest negative sensitivity coefficient for E_{min} and almost all the other sensible reactions were related to H, OH and O radicals. Meanwhile, the reactions concerned with NH_3 decomposition and N_2 formation all had positive sensitivity coefficients, due to the endothermicity that led to the decrease of H, OH and O. Moreover, the two major H_2O-generating reactions $OH + H_2 = H + H_2O$ and $NH_3 + OH = NH_2 + H_2O$, possessed similar in magnitude but opposite sensitivity coefficients. When H_2O acted as a three-body, the reaction $H + O_2 (+H_2O) = HO_2 (+H_2O)$ was insensitive to E_{min}. To summarize, the chemical effect induced by water addition primarily affected E_{min} by changing the concentrations of the radicals, mainly though reaction $O_2 + H = OH + O$, rather than directly participating in reactions (including as a three-body). This conclusion was manifested by the distributions of H, O and OH radicals under different humidification conditions shown in Fig. 3, where the peak mole fractions of H, O and OH all decreased as water content was increased.

3.2. Radiation effect on E_{min}

Next, the radiation effects on the ignition process of $NH_3/H_2/H_2O/O_2/N_2$ are discussed. Figure 5 shows the distributions of temperature T, chemical heat release rate Q and volumetric radiative power Q_R calculated by ADI, OTM and SNB models for Case WL3 when $R_f = 0.12$ cm. At the far upstream (center of the spherical flame, $r = 0$ cm), OTM- and SNB-obtained temperatures were both lower than that of ADI (by about 120 K), due to the radiative heat loss in the high temperature region (reflected by the red Q_R curves in Fig. 5). Subsequently, the radiation-induced decrease of temperature slowed down the reactions during the ignition process and suppressed the heat release. In terms of the comparison between the different radiation models (OTM and SNB), the radiation reabsorption effect considered in SNB reduced the radiative heat loss of the high-temperature burnt region ($r < 0.12$ cm) and preheated the cold unburned region (see the negative volumetric radiative energy at $r > 0.23$ cm for SNB), thus affected the flame structure and resulted in lower heat release rate in the SNB results Consequently, more ignition energy was required when radiation effect was fully considered. This was consistent with the simulated E_{min} results in Fig. 1, i.e., $E_{min,SNB} > E_{min,OTM} > E_{min,ADI}$. Furthermore, radiation effects on E_{min} as a function of humidification degree are depicted in Fig. 6. As the H_2O content in the mixture increased from 0% (Case WL0) to 9.63% (Case WL3), the normalized differences of E_{min} between OTM/SNB and ADI results increased from 1.64% to 16.47% and from 3.28% to 17.65%, respectively.

In order to elaborate the specific mechanism of radiation effect on E_{min} (under different conditions of humidification), analyses are conducted from various aspects. The radiative energy loss (i.e., the thermal effect) was firstly examined because of its most direct and profound influence on the E_{min}. As shown with the radiative powers in Fig. 5, the radiation heat loss calculated by OTM led to an obvious outward energy emission in the high-temperature burnt region, reducing the temperature of the ignition kernel and increasing the E_{min}. However, in the SNB result, even though the radiative heat loss in the burnt region was lower than that in the OTM result (since SNB additionally considered the internal radiative absorption and thus the radiative heat loss was no longer overestimated as by OTM), the temperature of the ignition kernel was still lower than that obtained by OTM, which was also reflected by the E_{min} results in Fig. 1, $E_{min,SNB} > E_{min,OTM}$. The reason was that radiation reabsorption of SNB relocated the area that emitted energy outwards when compared with the radiation heat loss of OTM: the radiative power in the SNB simulation exceeded that in the OTM after $r = 0.14$ cm (see Fig. 5). To this direction, radiative

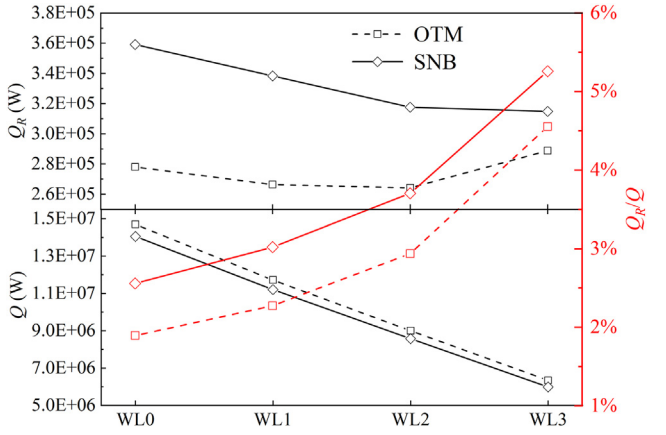

Fig. 7. Volumetric integrations of the radiative heat losses Q_R, the heat release rates Q and the ratios Q_R/Q calculated by the OTM and SNB models for all the cases when R_f = 0.12 cm.

heat losses and chemical heat releases should be integrated volumetrically and normalized for further evaluation.

As shown in Fig. 7, the integrated radiative power Q_R obtained by SNB was greater than that by OTM for all simulated conditions. The amount of radiation energy was affected by two factors, temperature and radiative properties (related to the concentrations of radiative species NH_3 and H_2O). On one hand, the temperature decreased with increased water content due to the high specific heat capacity of H_2O and dilution of combustibles, which should have resulted in nearly linear reduction of Q_R (as a function of H_2O fraction) from Case WL0 to WL3 for both OTM and SNB models. On the other hand, the increased water content, a strongly radiating species, also led to an increase in the averaged emissivity of the mixture that enhanced the emission outwards. Hence, Q_R of the OTM exhibited a turning point at somewhere between Cases WL2 and WL3. In contrast, in the SNB model the absorption coefficient was also promoted by the increase of water content, and thus the increase of radiative heat loss Q_R induced by more water was lower than that of OTM. Therefore, Q_R of SNB had a less reduction from Case WL2 to WL3. Moreover, to evaluate the influence of radiative heat loss Q_R on the total deposition energy, Q_R is further normalized by the heat release rates Q in Fig. 7. The thermal effect was more influential under high humidification conditions (monotonically increased from 1.89% to 4.55% for OTM and 2.56% to 5.26% for SNB, a trend similar to the radiation effect on E_{min} in Fig. 6).

Besides the aforementioned radiative heat loss (thermal effect), the reduction of energy generation (chemical effect, characterized by the chemical heat release rate Q) was another important factor that increased E_{min} when radiation was considered. As indicated by the volumetrically integrated heat release in Fig. 8, the chemical heat release calculated by OTM and SNB were both lower than that by ADI. This was due to the deceleration of chemical reactions caused by radiation-induced temperature drop (shown in Fig. 5). For the same reason, the chemical heat release rate Q at the flame front of SNB was lower than that of OTM, since the SNB-result had lower temperature in the reaction zone (r = 0.12 cm) as discussed above. The reduced exothermicity at the flame kernel led to an increase in the required external energy input to maintain self-propagation of the flame, and hence the required E_{min} under different radiative assumptions were $E_{min,SNB} > E_{min,OTM} > E_{min,ADI}$.

Furthermore, as per the aforementioned discussion on sensitivity analysis of E_{min}, the concentrations of H, OH and O radicals played important roles in controlling the ignition process and determining E_{min}. Figure 9 shows the concentrations of H, OH and O at the flame front calculated by the different radiation models

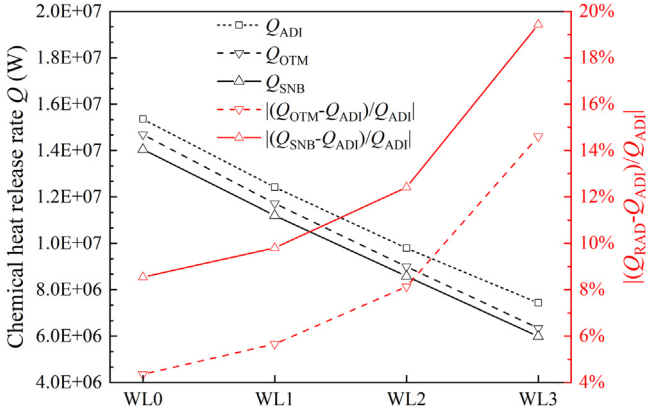

Fig. 8. Volumetric integrations of the heat release rates calculated by ADI, OTM and SNB models and the relative errors for all the cases when R_f = 0.12 cm.

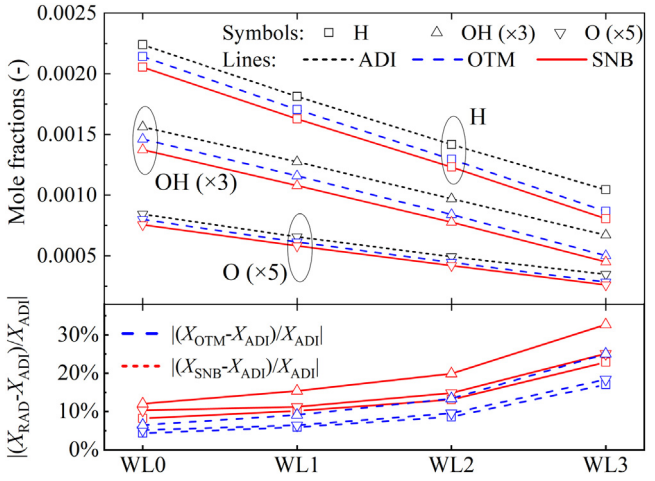

Fig. 9. Mole fractions of key radicals (H, OH and O) at the flame front for all the cases when R_f = 0.12 cm.

under different humidification conditions. H was the most abundant in all cases, which resulted in the highest sensitivity coefficient of the H-consumption reaction $O_2 + H = OH + O$ for E_{min}. The concentrations of H, OH and O all decreased after considering radiation heat loss and were further reduced by radiation reabsorption in the SNB results (see Fig. 7). Hence, in Fig. 8 chemical heat releases were suppressed and E_{min} became larger. The absolute relative differences of chemical heat release rates and radical concentrations between ADI and OTM/SNB (shown in Figs. 8 and 9, respectively) both increased with higher water content (e.g., OH from 12.05% for ADI to 32.68% for SNB). This manifested that the radiation-induced chemical effect was strengthened continuously (consistent with the variation of relative differences of chemical heat release rates Q in Fig. 8), leading to higher E_{min} when water content was increased.

Figure 10 shows the flame thickness (defined as $(T_b - T_u)/\max|dT/dr|$ in [33]) calculated by ADI, OTM and SNB for all the cases of Table 1 with R_f = 0.12 cm. As radiation heat loss was considered by OTM, its flame thickness increased compared to that of ADI, with their maximum absolute relative difference $|(\delta_{OTM} - \delta_{ADI})/\delta_{ADI}|$ up to 17.88% of WL3. The diffusion time became longer due to the increased flame thickness [34], which also led to the reduction of chemical heat release at the flame front (r = 0.12 cm). Hence, E_{min} required in the OTM simulations increased compared to those with ADI.

The consideration of radiation reabsorption further complicated the flame structure. On the one hand, the radiation reabsorption

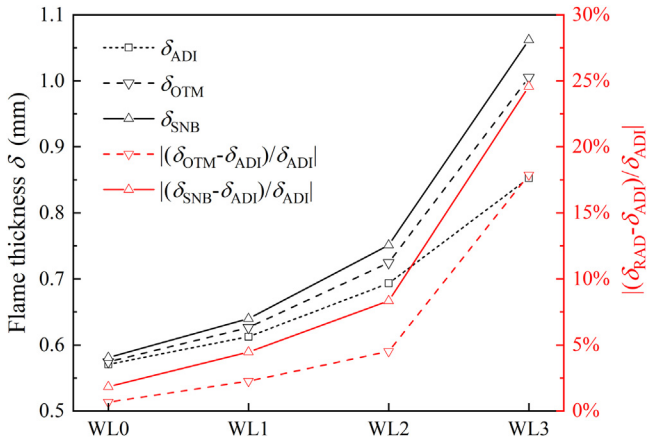

Fig. 10. Flame thickness calculated by different radiation models for all the cases when $R_f = 0.12$ cm.

considered by SNB corrected the overestimated radiation heat loss of OTM, and thus the temperature difference ($T_b - T_u$) of the SNB result was lower than that of OTM (shown in Fig. 5), which should have reduced δ. However, on the other hand, due to the radiation reabsorption effect considered in the SNB simulation, the low-temperature unburned region absorbed thermal radiation emitted from the high-temperature burnt region. Therefore, temperature of the unburnt region calculated by SNB was higher than those by OTM and ADI, and the reaction-diffusion zone of SNB was also larger than those of OTM and ADI, which further enlarged the flame thickness and delayed fuel diffusion to the reaction region. Finally, the radiation effects on flame thickness δ shown in Fig. 10 all increased with water content, which was consistent with the trend of relative difference of E_{min} shown in Fig. 6.

4. Conclusions

In this study, numerical simulations of the ignition process were conducted using different radiation models (ADI, OTM and SNB) for premixed $NH_3/H_2/H_2O/O_2/N_2$ mixtures with different degrees of humidification. The effects of humidification and radiation (including both radiation heat loss and reabsorption) on E_{min} were evaluated. The main conclusions were summarized as follow

(1) Humidification increased E_{min} and reduced the flammability of NH_3/H_2 fuels. The water content of 9.63% (vol.) resulted in a nearly 40% increase in E_{min} under adiabatic condition, which was even aggravated to ~60% when radiation was taken into consideration. Sensitivity analysis indicated that the chemical effect of water addition primarily affected E_{min} by changing the concentrations of radicals, mainly though the step $O_2 + H = OH + O$, rather than directly participating in reactions or indirectly as a three-body.

(2) The inclusion of both radiation heat loss (in OTM) and reabsorption (in SNB) caused higher E_{min} compared to the ADI results. As water (a strong radiating species) was increased, the radiation effects on E_{min} increased correspondingly. The radiation effect on E_{min}, quantified by the relative difference between $E_{min,OTM}/E_{min,SNB}$ and $E_{min,ADI}$, were up to 16.47% in OTM and 17.65% in SNB for Case WL3, respectively.

(3) Radiation affected E_{min} of $NH_3/H_2/H_2O/O_2/N_2$ mixtures mainly through thermal effect, chemical effect, which in turn also altered the flame structures. The outward energy emission by the radiation models (i.e., thermal effect) reduced the ignition kernel temperature and increased E_{min}. Meanwhile, the reduced temperature decelerated the rates of chemical reactions, which further led to the decrease of H, OH and O radicals and internal energy deposition in the reaction zone. The radiation effect on flame structure was reflected by the change in flame thickness. The radiation reabsorption resulted in a wider reaction-diffusion region, which thickened the flame and slowed down the fuel diffusion to the reaction region, and eventually caused $E_{min,SNB} > E_{min,OTM}$.

Declaration of Competing Interest

The authors declare that they have no known competing financial interests or personal relationships that could have appeared to influence the work reported in this paper.

Acknowledgments

This research was supported by the National Key Research Development Program of China (no. 2022YFB4003901), the National Natural Science Foundation of China (nos. 52276185, 52276189 and 52206157) and the Fundamental Research Funds for the Central Universities (nos. 2020JG005, 2020DF01). RS in addition acknowledges support from NSFC through a National Talent Program.

References

[1] J. Witte, Power to Ammonia, Feasibility Study for the Value Chains and Business Cases to Produce CO_2-Free Ammonia Suitable for Various Market Applications, Institute for Sustainable Process Technology (ISPT), Amersfoort, The Netherlands, 2017 Report no. TESI115001.
[2] J.S. Cardoso, V. Silva, R.C. Rocha, M.J. Hall, M. Costa, D. Eusébio, Ammonia as an energy vector: current and future prospects for low-carbon fuel applications in internal combustion engines, J. Cleaner Prod. 296 (2021) 126562.
[3] F.J. Verkamp, M.C. Hardin, J.R. Williams, Ammonia combustion properties and performance in gas-turbine burners, Symp. (Int.) Combust. 11 (1967) 985–992.
[4] E.C. Okafor, Y. Naito, S. Colson, A. Ichikawa, T. Kudo, A. Hayakawa, H. Kobayashi, Measurement and modelling of the laminar burning velocity of methane-ammonia-air flames at high pressures using a reduced reaction mechanism, Combust. Flame 204 (2019) 162–175.
[5] A. Valera-Medina, R. Marsh, J. Runyon, D. Pugh, P. Beasley, T. Hughes, P. Bowen, Ammonia–methane combustion in tangential swirl burners for gas turbine power generation, Appl. Energy 185 (2017) 1362–1371.
[6] O. Mathieu, E.L. Petersen, Experimental and modeling study on the high-temperature oxidation of ammonia and related NOx chemistry, Combust. Flame 162 (2015) 554–570.
[7] H. Lesmana, M. Zhu, Z. Zhang, J. Gao, J. Wu, D. Zhang, An experimental investigation into the effect of spark gap and duration on minimum ignition energy of partially dissociated NH_3 in air, Combust. Flame 241 (2022) 112053.
[8] J. Li, H. Huang, N. Kobayashi, Z. He, Y. Nagai, Study on using hydrogen and ammonia as fuels: combustion characteristics and NOx formation, Int. J. Energy Res. 38 (2014) 1214–1223.
[9] D. Pugh, P. Bowen, A. Valera-Medina, A. Giles, J. Runyon, R. Marsh, Influence of steam addition and elevated ambient conditions on NOx reduction in a staged premixed swirling NH_3/H_2 flame, Proc. Combust. Inst. 37 (2019) 5401–5409.
[10] E. Mastorakos, Ignition of turbulent non-premixed flames, Prog. Energy Combust. Sci. 35 (2009) 57–97.
[11] K. Takizawa, N. Igarashi, S. Takagi, K. Tokuhashi, S. Kondo, Quenching distance measurement of highly to mildly flammable compounds, Fire Saf. J. 71 (2015) 58–68.
[12] H. Lu, F. Liu, K. Wang, G. Xu, H.J. Curran, Numerical study on the minimum ignition energy of a methane-air mixture, Fuel 285 (2021) 119230.
[13] C. Wu, R. Schießl, U. Maas, Numerical studies on minimum ignition energies in methane/air and iso-octane/air mixtures, J. Loss Prev. Process Ind. 72 (2021) 104557.
[14] W. Zhang, Z. Chen, W. Kong, Effects of diluents on the ignition of premixed H_2/air mixtures, Combust. Flame 159 (2012) 151–160.
[15] W. Zhang, X. Gou, Z. Chen, Effects of water vapor dilution on the minimum ignition energy of methane, n -butane and n -decane at normal and reduced pressures, Fuel 187 (2017) 111–116.
[16] S. Zheng, H. Liu, R. Sui, B. Zhou, Q. Lu, Effects of radiation reabsorption on laminar NH_3/H_2/air flames, Combust. Flame 235 (2022) 111699.
[17] S. Zheng, R. Sui, W. Liang, H. Zhou, C.K. Law, On band lumping, radiation reabsorption, and high-pressure effects in laminar flame propagation, Combust. Flame 221 (2020) 86–93.
[18] S. Zheng, H. Liu, Y. He, Y. Yang, R. Sui, Q. Lu, Combustion of biomass pyrolysis gas: roles of radiation reabsorption and water content, Renew. Energy 205 (2023) 864–872.
[19] Z. Chen, Studies on the initiation, propagation, and extinction of premixed flames, Princeton University, 2009.

[20] Z. Chen, Effects of hydrogen addition on the propagation of spherical methane/air flames: a computational study, Int. J. Hydrogen Energy 34 (2009) 6558–6567.
[21] Z. Chen, M.P. Burke, Y. Ju, Effects of Lewis number and ignition energy on the determination of laminar flame speed using propagating spherical flames, Proc. Combust. Inst. 32 (2009) 1253–1260.
[22] Z. Chen, M.P. Burke, Y. Ju, Effects of compression and stretch on the determination of laminar flame speeds using propagating spherical flames, Combust. Theor. Model. 13 (2009) 343–364.
[23] Z. Chen, X. Qin, B. Xu, Y. Ju, F. Liu, Studies of radiation absorption on flame speed and flammability limit of CO_2 diluted methane flames at elevated pressures, Proc. Combust. Inst. 31 (2007) 2693–2700.
[24] Z. Chen, M.P. Burke, Y. Ju, On the critical flame radius and minimum ignition energy for spherical flame initiation, Proc. Combust. Inst. 33 (2011) 1219–1226.
[25] A. Frendi, M. Sibulkin, Dependence of minimum ignition energy on ignition parameters, Combust. Sci. Technol. 73 (1990) 395–413.
[26] S.J. Young, Nonisothermal band model theory, J. Quant. Spectrosc. Radiat. Transfer 18 (1977) 1–28.
[27] P. Rivière, A. Soufiani, Updated band model parameters for H_2O, CO_2, CH_4 and CO radiation at high temperature, Int. J. Heat Mass Transfer 55 (2012) 3349–3358.
[28] I.E. Gordon, L.S. Rothman, C. Hill, R.V. Kochanov, Y. Tan, P.F. Bernath, M. Birk, V. Boudon, A. Campargue, K.V. Chance, B.J. Drouin, J.M. Flaud, R.R. Gamache, J.T. Hodges, D. Jacquemart, V.I. Perevalov, A. Perrin, K.P. Shine, M.A.H. Smith, J. Tennyson, G.C. Toon, H. Tran, V.G. Tyuterev, A. Barbe, A.G. Császár, V.M. Devi, T. Furtenbacher, J.J. Harrison, J.M. Hartmann, A. Jolly, T.J. Johnson, T. Karman, I. Kleiner, A.A. Kyuberis, J. Loos, O.M. Lyulin, S.T. Massie, S.N. Mikhailenko, N. Moazzen-Ahmadi, H.S.P. Müller, O.V. Naumenko, A.V. Nikitin, O.L. Polyansky, M. Rey, M. Rotger, S.W. Sharpe, K. Sung, E. Starikova, S.A. Tashkun, J.V. Auwera, G. Wagner, J. Wilzewski, P. Wcisło, S. Yu, E.J. Zak, The HITRAN2016 molecular spectroscopic database, J. Quant. Spectrosc. Radiat. Transfer 203 (2017) 3–69.
[29] S. Zheng, Y. He, B. Hu, J. Zhu, B. Zhou, Q. Lu, Effects of radiation reabsorption on the flame speed and NO emission of NH_3/H_2/air flames at various hydrogen ratios, Fuel 327 (2022) 125176.
[30] S. Zheng, H. Liu, D. Li, Z. Liu, B. Zhou, Q. Lu, Effects of radiation reabsorption on the laminar burning velocity of methane/air and methane/hydrogen/air flames at elevated pressures, Fuel 311 (2022) 122586.
[31] S. Zheng, H. Liu, Q. Li, J. Zhu, M. Sun, B. Zhou, R. Sui, Q. Lu, Effects of radiation reabsorption on the laminar flame speed and NO emission during aviation kerosene combustion at elevated pressures, Fuel 324 (2022) 124545.
[32] K.P. Shrestha, C. Lhuillier, A.A. Barbosa, P. Brequigny, F. Contino, C. Mounaïm-Rousselle, L. Seidel, F. Mauss, An experimental and modeling study of ammonia with enriched oxygen content and ammonia/hydrogen laminar flame speed at elevated pressure and temperature, Proc. Combust. Inst. 38 (2021) 2163–2174.
[33] C.K. Law, C.J. Sung, Structure, aerodynamics, and geometry of premixed flamelets, Prog. Energy Combust. Sci. 26 (2000) 459–505.
[34] H.H. Kim, S.H. Won, J. Santner, Z. Chen, Y. Ju, Measurements of the critical initiation radius and unsteady propagation of n-decane/air premixed flames, Proc. Combust. Inst. 34 (2013) 929–936.